

Localized Orbital Description of Electronic Structure

Joydeep Bhattacharjee and Umesh V Waghmare

Theoretical Sciences Unit

Jawaharlal Nehru Centre for Advanced Scientific Research

Jakkur PO, Bangalore 560 064 India

We present a simple and general method for construction of localized orbitals to describe electronic structure of extended periodic metals and insulators as well as confined systems. Spatial decay of these orbitals is found to exhibit exponential behavior for insulators and power law for metals. While these orbitals provide a clear description of bonding, they can be also used to determine polarization of insulators. Within density functional theory, we illustrate applications of this method to crystalline Aluminium, Copper, Silicon, PbTiO₃ and molecules such as ethane and diborane.

PACS numbers: 71.15.-m 71.20.-b 71.23.An

Localized orbitals, such as Wannier functions[1], have played an important role in many aspects of quantum mechanical description of electrons in solids and molecules. They highlight atomic character of electrons[2] and elucidate the nature of bonding. Their spatial localization makes them useful as basis functions for efficient calculations of electronic structure that scale linearly with system size[3, 4, 5]. They are often useful in the construction of lattice model Hamiltonians for structural transitions[6] as well as strongly correlated systems[7]. Wannier functions are intimately related to geometric phases of Bloch electron[8, 9] and electric polarization of insulators[10, 11]. Recent surge of interest in Wannier functions is due to their use in modeling transport [12] and electric field dependent properties of periodic solids.

Many schemes for construction of localized or Wannier orbitals have been presented over the last four decades. To name a few, early works of Foster and Boys[13] were based on maximizing the dipole moment matrix elements between orthonormal orbitals making their centroids maximally apart from each other, followed by Reudenberg's [14] approach of maximizing the orbital self-repulsion energies. Kohn presented a scheme[2] for arriving at exponentially localized real orthonormal WFs through a variational principle for total energy. Maximally localized Wannier functions (MLWF)[15] were introduced by Marzari and Vanderbilt that minimize the variance of position operator \vec{r} , in a given subspace of states. For example, orbitals maximally localized in a spatial direction α (hermaphrodite orbitals[16]) are eigenfunctions of position operator r_α in the given subspace. As different components of \vec{r} do not commute when projected into a subspace, MLWFs are obtained through numerical minimization of variance of \vec{r} used as a measure of localization. MLWFs have been generalized to the cases of entangled bands[17] and to atom-centered orbitals[18].

WFs are Fourier transform of Bloch functions: $W(\mathbf{r}) = \int d\mathbf{k} e^{i\mathbf{k}\cdot\mathbf{r}} \psi_{\mathbf{k}}(\mathbf{r})$. Due to freedom in \mathbf{k} -dependent phase factor accompanying $\psi_{\mathbf{k}}$, WFs are non-unique. Smoothness of these phases determine localization properties of

WFs. MLWFs in 1-dimension can be obtained simply (*with out* a variational calculation) through construction of Bloch states that are smooth (generated using parallel transport along \mathbf{k}) and periodic in k -space[9]. Generalization of this idea to three dimensions is not readily possible, as the smoothness and periodicity of Bloch states as a function of k_α achieved through parallel transport along one direction is disturbed by that along another direction in k -space. Here, we provide a solution by connecting Bloch states at different \mathbf{k} 's by parallel transport along paths that run *outside* the \mathbf{k} -space. Resulting Bloch functions are periodic and optimally smooth in all directions in k -space, whose Fourier transform yields well localized Wannier functions. It is efficient and simple because it avoids a variational calculation and issues of local minima. Its versatility is demonstrated through applications to insulators, metals and molecules.

In the first step of this method, we develop an *auxiliary subspace* of highly localized orthonormal orbitals with desired symmetry properties described by (a) center of the orbital (Wyckoff site) $\{\tau_\kappa\}$ and (b) irreducible representation (irrep) of its site symmetry group according to which it transforms[2, 19]. This choice can be guided through symmetry analysis of Bloch states[6, 8, 20] in the *physical subspace* of occupied states. For simplicity, we use Gaussian form for the radial part and a spherical harmonic corresponding to the irrep of localized orbitals:

$$\Psi_\mu(\mathbf{R}, \mathbf{r}) = (\alpha/2\pi)^{3/2} e^{-\alpha|\mathbf{r}-\tau_\kappa-\mathbf{R}|^2} Y_{lm}(r - \widehat{\tau_\kappa} - R) \quad (1)$$

where α determines the width of the Gaussian, \mathbf{R} is a direct space lattice vector and μ is an orbital index. α is chosen to be large enough to keep orbitals in neighbouring unit cells orthogonal. Cell periodic part $v_{\mu\mathbf{k}}$ of Bloch functions spanning the auxiliary subspace is given by Fourier transform:

$$\langle \mathbf{r} | v_{\mu\mathbf{k}} \rangle = \sum_{\mathbf{R}} e^{i\mathbf{k}\cdot(\mathbf{R}-\mathbf{r})} \Psi_\mu(\mathbf{R}, \mathbf{r}) \quad (2)$$

We note that $\{ \langle \mathbf{r} | v_{\mu\mathbf{k}} \rangle \}$ are smooth as a function of \mathbf{k} and satisfy $|v_{\mu\mathbf{k}}\rangle = |v_{\mu\mathbf{k}+\mathbf{G}}\rangle$, \mathbf{G} being a reciprocal lattice vector.

In the second step, we perform a unitary transformation of Bloch states in the physical subspace (eg. energy eigenfunctions of occupied states) such that the open path[21] non-abelian geometric phases between states in physical and auxiliary subspaces at fixed \mathbf{k} vanish. Overlap matrix $S_{\mu n}^{\mathbf{k}} = \langle u_{\mu\mathbf{k}} | u_{n\mathbf{k}} \rangle$, where $|u_{n\mathbf{k}}\rangle$ is cell periodic part of energy an eigen state, relates to geometric phase matrix $\Gamma_{\mathbf{k}}$ through:

$$S^{\mathbf{k}} = R_{\mathbf{k}} e^{i\Gamma_{\mathbf{k}}}, \quad (3)$$

where R is a positive definite Hermitian matrix. Determination of R and $\Gamma_{\mathbf{k}}$ is accomplished using singular value decomposition of S :

$$S^{\mathbf{k}} = U_{\mathbf{k}} \Sigma_{\mathbf{k}} V_{\mathbf{k}}^{\dagger} \quad (4)$$

where $\Sigma_{\mathbf{k}}$ is a diagonal matrix with non-negative singular values in its diagonal. Vanishing of singular value(s) at some \mathbf{k} signals a non-optimal choice of symmetries of localized orbitals in the auxiliary subspace and the need for correction. Using Eqn.4, $R_{\mathbf{k}} = U_{\mathbf{k}} \Sigma_{\mathbf{k}} U_{\mathbf{k}}^{\dagger}$ and $e^{i\Gamma_{\mathbf{k}}} = U_{\mathbf{k}} V_{\mathbf{k}}^{\dagger}$. A unitary transformation on the $\{u_{n\mathbf{k}}\}$ given by a matrix $M_{\mathbf{k}} = (U_{\mathbf{k}} V_{\mathbf{k}}^{\dagger})^*$ transforms the overlap matrix $S^{\mathbf{k}}$ to a hermitian form,

$$\tilde{S}^{\mathbf{k}} = S^{\mathbf{k}} (V_{\mathbf{k}} U_{\mathbf{k}}^{\dagger}) = U_{\mathbf{k}} \Sigma_{\mathbf{k}} U_{\mathbf{k}}^{\dagger},$$

corresponding to vanishing geometric phases.

A sketch in terms of paths that connect physical and auxiliary subspaces (shown in Fig 1) enables understanding of our method. Closed paths parametrized by \mathbf{k} , such as C , in the physical subspace can have nontrivial geometric phases which forbid construction of smooth functions by parallel transport along \mathbf{k} within the physical subspace. In the present method, we make use of paths, labeled as P , to connect states at two \mathbf{k} 's in the physical space. For $\mathbf{k} = \text{constant}$ segments of path P (dashed lines), geometric phases are made to vanish. Secondly, geometric phases along any closed path parametrized by \mathbf{k} in the auxiliary subspace vanish. Hence, Bloch functions in the physical subspace transformed with $M_{\mathbf{k}}$ have a single valued and periodic phase as a function of \mathbf{k} .

We include occupation numbers $f_{n\mathbf{k}}$ while transforming energy eigenfunctions and obtain

$$|\tilde{u}_{\mu\mathbf{k}}\rangle = \sum_j M_{\mu j} |u_{j\mathbf{k}}\rangle f_{n\mathbf{k}}^{1/2}, \quad (5)$$

which are periodic in \mathbf{k} by construction and the random phases accompanying $\{u_{n\mathbf{k}}\}$ are filtered out in this procedure. Localized orbitals are obtained by Fourier transforming $\{\tilde{u}_{\mu\mathbf{k}}(\mathbf{r})\}$:

$$\langle \mathbf{r} | \Phi_{\mu}(\mathbf{R}) \rangle = \frac{\Omega}{(2\pi)^3} \sum_{\mathbf{k}} e^{i(\mathbf{k}-\mathbf{R}) \cdot \mathbf{r}} \langle \mathbf{r} | \tilde{u}_{\mu\mathbf{k}} \rangle \quad (6)$$

where Ω is the unit cell volume. Localization of $|\Phi_{\mu}(\mathbf{R})\rangle$ is determined by the ‘‘smoothness’’ of $\{\tilde{u}_{\mu\mathbf{k}}(\mathbf{r})\}$, which

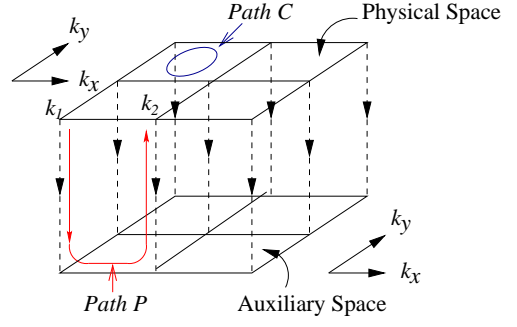


FIG. 1: Two horizontal planes are used to display physical and auxiliary subspaces, in which the member functions are parametrized with k_x and k_y . Dashed lines indicate paths connecting states at a given \mathbf{k} in physical subspace with those in the auxiliary subspace.

depends on the precise location of centre and symmetry properties of localized orbitals in the auxiliary subspace. A quantitative idea of the *smoothness* is obtained with the Berry connection matrix $B_{\alpha}(k)$:

$$B_{\alpha}^{\mu\nu}(k) = -Im \langle \tilde{u}_{\mu\mathbf{k}} | \frac{\partial}{\partial k_{\alpha}} | \tilde{u}_{\nu\mathbf{k}} \rangle, \quad (7)$$

and its Fourier components. If the matrix $B_{\alpha}(k)$ is diagonal and its diagonal entries are constant as a function of k_{α} (it has vanishing Fourier components for $\mathbf{R} \neq 0$), Φ_{μ} are maximally localized in α direction[9, 16]. For the systems studied in this work, diagonal elements of B are found to be constant as a function of k , indicating good localization properties of Φ_{μ} .

We note that functions $|\Phi_{\mu}(\mathbf{R})\rangle$ are *not* maximally localized[15] by construction. However, if desired, the MLWFs can be readily obtained through a single step of maximal joint diagonalization[22] of the three components of position operators in Φ -basis:

$$\langle r_{\alpha} \rangle_{\mu, \mu', R_1, R_2} = \int_{\Omega N_{k_{\alpha}}} \Phi_{\mu}^*(\mathbf{R}_1, \mathbf{r}) r_{\alpha} \Phi_{\mu'}(\mathbf{R}_2, \mathbf{r}) d\mathbf{r}, \quad (8)$$

Electronic part of electric polarization is obtained using:

$$P_{\alpha}^{el} = \frac{q}{\Omega} \sum_{\mu} \langle \Phi_{\mu}(\mathbf{R} = \mathbf{0}) | r_{\alpha} | \Phi_{\mu}(\mathbf{R} = \mathbf{0}) \rangle. \quad (9)$$

Inclusion of occupation numbers in Eqn 5 ensures a simple and general form for density matrix $\rho(r, r') = \sum_{R, \mu} \langle r | \Phi_{\mu}(R) \rangle \langle \Phi_{\mu}(R) | r' \rangle$. As the present analysis at \mathbf{k} is decoupled from that at other \mathbf{k} 's, it applies equally well to simple, compound and entangled bands, and can be performed efficiently on a parallel computer. For molecules or confined systems treated within periodic boundary conditions, it can be readily applied using a single $\mathbf{k} = (000)$ point; it equally well applies to confined systems treated with open boundary conditions. In the present scheme, construction of atom-centered orbitals[18] for covalent systems necessitates expansion of

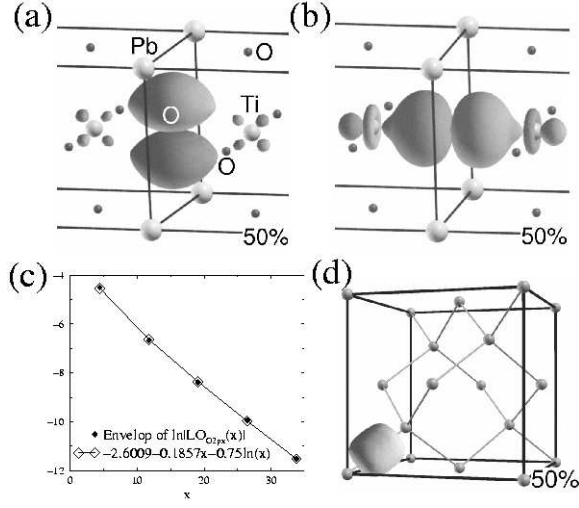


FIG. 2: (a) and (b) shows $2p_y$ and $2p_x$ orbitals respectively of a bridging oxygen in PbTiO_3 . (c) shows the nature of decay of the $2p_x$ orbital shown in (b). (d) shows a bond centered orbital representing the Si-Si σ -bond in bulk Si.

the physical subspace to include anti-bonding bands. It is somewhat similar to physically intuitive derivation of Wannier functions in Ref.23.

We illustrate our method within density functional theory through applications to insulators, metals and molecules. The energy eigen states, which are the main inputs to our method, are calculated using ABINIT implementation[24] of density functional theory and norm-conserving pseudopotentials. We use Monkhorst Pack meshes (finer than a $9 \times 9 \times 9$ mesh) of k-points to sample Brillouin zones. Isosurfaces of localized orbitals (indicating isovalue as percentage of its maximum in figures) have been generated using a visualization software XcrysDen[25].

For PbTiO_3 in the cubic perovskite structure, symmetry of occupied bands implies the choice of atom-centered orbitals: Pb-centered (s - and d -like), Ti-centered (s - and p -like) and O-centered (s - and p -like). Oxygen centered localized orbitals with p symmetry form two groups: (a) ones perpendicular to the -O-Ti-O- chain (Fig.2.(a)), (b) ones along the -O-Ti-O- chain (Fig.2.(b)). A former has π -like overlap with d_{xy} orbital of Ti and a variance of 1.44 \AA^2 , while the latter has σ -like overlap with d_{x^2} orbital of Ti and a smaller variance of 1.14 \AA^2 . For an O-centered orbital with s symmetry, we get a variance of 0.54 \AA^2 (compared with 0.52 \AA^2 of Ref. [26]). We determined Born effective charge (Z^*) of Ti using $Z^* = \Omega \Delta P_\alpha / \Delta d_\alpha$, where Δd_α is a small displacement of Ti atom that changes the net polarization ($P_\alpha = P_\alpha^{\text{ion}} + P_\alpha^{\text{el}}$) by ΔP_α . Our estimate of $Z^*(\text{Ti}) = 7.02$ agrees well with a linear response calculation[24], with contribution from each O-centered p orbital in group (a) and (b) of 1.6 and 0.8 respectively. Our estimate of

$Z^*(\text{Pb}) = 3.86$, also in good agreement with the linear response result, has a contribution of 1.4 from O-centered orbitals in Ti-O planes. Spatial decay of an O-centered orbital in group (b), shown in Fig. 2(c), exhibits a power law times times exponential form[2]. The power-law exponent obtained from a fit is -0.75 , consistent with a theoretical prediction[27]. We confirmed that the diagonal elements of the Berry connection matrix (Eqn.7 do not change with \mathbf{k} , indicating individually maximal localization of these orbitals.

For Si in diamond structure, a covalent semiconductor, we illustrate construction of bond and atom centered orbitals corresponding to different choices of subspaces. Symmetries of Bloch states in the occupied subspace ($D=4$) dictate a choice of bond-centered orbital with full site symmetry. Corresponding bond centered orbitals (shown in Fig.2.(d)) have a variance of 2.2 \AA^2 (compared with 2.05 \AA^2 of an MLWF[15]) each. We find that the diagonal elements of Berry connection matrix are indeed constant as a function of k , implying maximal localization of an orbital individually. In the construction of atom-centered orbitals we use double the number of bands in physical subspace, and atom-centered orbitals with s and p symmetry. Our scheme provides two options: (a) treat silicon as a metal (using occupation numbers in Eqn.5), which generates nonorthonormal atom-centered orbitals which exactly span the occupied subspace, and (b) not use occupation numbers, which generates orthonormal atom-centered orbitals that span the occupied as well as unoccupied states. The former can be important in studies of bonding, whereas the latter could be useful as basis in $O(N)$ methodology.

We illustrate localized orbitals in metallic systems characterized by multi-centered bonding, *ie.* sharing of electrons among more than two atoms, with examples of Cu and Al in the FCC crystal structure. Due to partial

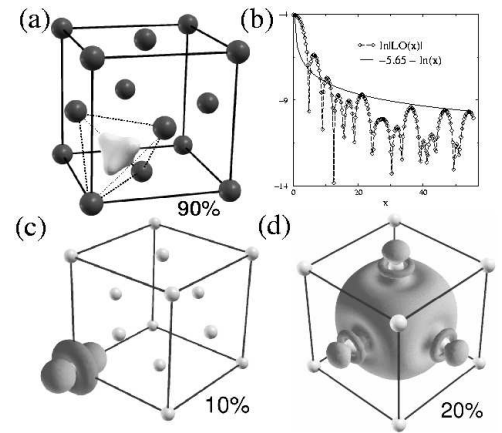


FIG. 3: Localized orbitals of metals: an orbital centered at the tetrahedral site of Al (a), and its spatial decay (b); atom centered LO with $3d_{z^2}$ symmetry (c) and an LO centered at the octahedral site of Cu (d).

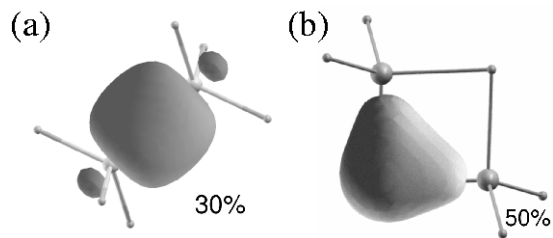


FIG. 4: (a) shows a bond centered orbital representing the C-C σ -bond in C_2H_6 . (b) shows the B-H-B three center bond in B_2H_6 .

occupancy of bands in metals, the dimensionality of auxiliary subspace is taken to be greater than largest number of occupied bands at any \vec{k} , the same as the number of energy bands calculated in DFT calculation with temperature smearing used for occupation numbers. In the case of Al, we used (guided by symmetry and singular values) spherically symmetric orbitals centering at the tetrahedral sites $(1, 1, 1)\frac{a}{4}$ in addition to atom-centered s -like orbital to construct an auxiliary subspace. From normalization, we find each localized orbital centered at the tetrahedral site (Fig.3.(a)) and the atomic site to be occupied with $1.2e$ and $0.6e$ respectively. The former provides 4-centered directional bonding among the four Al atoms equidistant from its center. Its spatial decay (shown in Fig.3.(b)) exhibits a power law decay with an exponent -1, consistent with earlier calculations[28] in the free electron limit. In the case of Cu, we used atom centered s - and d -like orbitals and an s -like orbital centered at octahedral site $O = (1, 1, 1)\frac{a}{2}$. Among atom-centered orbitals, a d -like orbital (Fig.3(c)) is quite localized and is occupied with $1.86e$, while the s -like orbital is occupied with $0.69e$. The orbital centered in the octahedral site (shown in Fig.3.(d)) is occupied with $1.01e$ providing a 6-centered bond, and exhibits slight mixing with atomic d -orbitals. Our results clearly reveal stronger directional bonding in Al than in Cu, which was also concluded from charge density analysis in understanding contrasting mechanical behavior of Al and Cu[29].

Finally, we demonstrate application of the present scheme to localized orbitals in C_2H_6 and B_2H_6 molecules. In the former, we have used bond-centered orbitals and in the latter, we use bond-centered orbitals for the BH_2 radicals and s -like orbitals centered on H atoms that bridge the two BH_2 radicals. C-C σ -bonding orbital (Fig.4(a)) has a variance of 0.83 \AA^2 , which reduces to 0.76 \AA^2 after joint diagonalization to obtain an MLWF. Orbitals corresponding to heteropolar C-H σ bonds have their centroids closer to the H atoms. The orbital centered on a bridging H atom of B_2H_6 (shown in Fig.4(b)) reveals the well-known three-centered bond, and has a variance of 0.96 \AA^2 each.

In conclusion, we have presented a simple method for construction of well localized orbitals, that is applicable

to extended metals and insulators as well as finite systems. While demonstrated here for electronic problems, it can be readily used in treatment of phonons. It should be useful for a large number of problems in condensed matter physics.

JB thanks CSIR, India for a research fellowship. UVW acknowledges support from the DuPont Young Faculty Award and the central computing facility at JNCASR, funded by the DST, Government of India.

-
- [1] G. Wannier, Phys. Rev. **52**, 191 (1937).
 - [2] W. Kohn, Phys. Rev. B **7**, 4388 (1973).
 - [3] J. M Soler *et al*, J. Phys.: Condens. Matter **14**, 2745-2779 (2002)
 - [4] G. Galli and M. Parrinello, Phys. Rev. Lett. **69**, 3574 (1992).
 - [5] S. Geodecker and L. Colombo, Phys. Rev. Lett. **73**, 122 (1994).
 - [6] K. M. Rabe and U. V. Waghmare, Phys. Rev. B **52**, 13236 (1995).
 - [7] E. Pavarini *et al*, Phys. Rev. Lett. **87**, 047003 (2001).
 - [8] J. Zak, Europhys. Lett. **9**, (7), pp. 615-620 (1989).
 - [9] J. Bhattacharjee and U. V. Waghmare, Phys. Rev. B **71**, 045106 (2005).
 - [10] R. D. King-Smith and D. Vanderbilt, Phys. Rev. B **47**, 1651 (1993).
 - [11] R. Resta, Rev. Mod. Phys. **66**, 899 (1994).
 - [12] A. Calzolari, et al, Phys. Rev. B **69**, 035108 (2004).
 - [13] J. M. Foster and S.F. Boys, Rev. Mod. Phys. **32**, 300 (1960).
 - [14] C. Edmiston and K. Ruedenberg, Rev. Mod. Phys. **35**, 457 (1963).
 - [15] N. Marzari and D. Vanderbilt, Phys. Rev. B **56**, 12 847 (1997).
 - [16] C. Sgiarovello, M. Peressi and R. Resta, Phys Rev **B64**, 115202 (2001).
 - [17] I. Souza, N. Marzari and D. Vanderbilt, Phys. Rev. B **65** 035109 (2001).
 - [18] Z. Li and D. S. Kosov, cond-mat/0507649.
 - [19] J. Des Cloizeux, Phys. Rev. **129**, 554 (1963)
 - [20] V. P. Smirnov and D. E. Usvyat, Phys. Rev. **B64**, 245108 (2001).
 - [21] J. Samuel and R. Bhandari, Phys. Rev. Lett. **60**, 2339 (1988).
 - [22] J. Cardoso and A. Souloumiac, (SIAM) J. Mat. Anal. Appl. **17**, 161 (1996).
 - [23] S. Satpathy and Z. Pawlowska, Phys. Stat. Sol. **b 145**, 555 (1988).
 - [24] The ABINIT software project, X. Gonze *etal*, Computational Materials Science **25**, 478-492 (2002).
 - [25] A. Kokalj, XCrySDen - a new program for displaying crystalline structures and electron densities, J. Mol. Graphics Modelling, **17**, 176 (1999).
 - [26] M. Veithen, X. Gonze, and Ph. Gosez, Phys. Rev. B **66**, 235113 (2002).
 - [27] L. He and D. Vanderbilt, Phys. Rev. Lett. **86**, 5341 (2001).
 - [28] S. Geodecker, Phys. Rev. B **58**, 583501 (1998)
 - [29] S. Ogata, J. Li and S. Yip, Science, **298**, 807 (2002).